Progress In Electromagnetics Research, Vol. 129, 215–229, 2012

EQUIVALENT CIRCUIT ANALYSIS OF RIDGE-LOADED FOLDED-WAVEGUIDE SLOW-WAVE STRUCTURES FOR MILLIMETER-WAVE TRAVELING-WAVE TUBES

Y. Hou*, J. Xu, H.-R. Yin, Y.-Y. Wei, L.-N. Yue, G.-Q. Zhao, and Y.-B. Gong

National Key Laboratory of Science and Technology on Vacuum Electronics, University of Electronic Science and Technology of China, Chengdu 610054, China

Abstract—In this paper, a new simple equivalent circuit model for analysis of dispersion and interaction impedance characteristics of ridge-loaded folded-waveguide slow-wave structure is presented. In order to make the computational results more accurately, the effects of the presence of the beam-hole and discontinuity due to the waveguide bend and the narrow side dimension change of this kind of structure were considered. The dispersion characteristics and the interaction impedance are numerical calculated and discussed. The analytical results agree very well with those obtained by the 3-D electromagnetic high-frequency simulation software. It is indicated that the equivalent circuit methods are reliable and high efficiency.

1. INTRODUCTION

The folded waveguide (FWG) slow-wave structure (SWS) is one of the most important millimeter and terahertz-wave amplifiers which are suitable for traveling-wave tubes (TWTs) [1–7]. As a full-metal structure, the FWG circuit has been shown to have excellent performances in lower RF loss, higher power handing capability and simple input and output circuit transitions. However, the previous investigations on FWG-TWTs reveal that their electron efficiency are relatively low, which are mainly limited by the beam-wave interaction impedance [8–13]. In order to increase the electron efficiency of this kind of structure, a novel structure, ridge-loaded folded-waveguide slow-wave structure (RLFWG-SWS), has been presented by our

Received 26 April 2012, Accepted 14 June 2012, Scheduled 21 June 2012

* Corresponding author: Yan Hou (houyan0308@163.com).

research group [14]. Although the boundary conditions are very complicated, we still made some rough analysis of this structure according to the field-matching method under the following conditions:

1) The reflections from the waveguide bend and the beam tunnel are negligible.
2) The RLFWG-SWS was straightened and an equivalent analytical model was adapted.

All these assumptions will bring some errors, which will further impact on the accuracy of the design of TWTs, especially influence on the dispersion characteristics which is more sensitive to predict the performance of TWTs. For the sake of studying this structure as accurate as possible, we seek to use other method to analyze the RLFWG-SWS. Just because of this reason, equivalent circuit model based on transmission line cascade network, which can be used to analyze the high frequency characteristics of RLFWG-SWS, has been proposed.

With respect to the equivalent circuit, some scholars have paid attention to it, such as Booske et al. [12], Liu [15], Na et al. [16], Han et al. [17] and Sumathy et al. [18]. Na et al. [16] and Han et al. [17] exclude the effect of the beam hole. A thorough equivalent circuit analysis of folded-waveguide slow-wave structure including the effect of the beam hole was proposed by Booske et al. [12]. By means of the high pass filter model, the analysis of the high-frequency characteristic of FWG-SWS has been developed by Sumathy et al. [18].

In this paper, a complete equivalent circuit model is developed for studying V-band RLFWG-SWS. As an import atmospheric attenuation window, the V-band has been shown great potential on both military and civil areas, especially for complex military communication and information countermeasure [19–21]. The frequency range of 60–65 GHz is a region of the millimeter-wave spectrum that has been designated for inter-satellite communications.

The dispersion properties and the beam-wave interaction impedance are calculated using equivalent circuit model and three-dimensional (3-D) high-frequency electromagnetic simulation software (HFSS) [22]. The effects of the beam hole, the discontinuity of waveguide bend and the change of the narrow side dimension are considered in our model. The analytical results agree well with those obtained by HFSS.

This paper is organized as follows. A brief introduction is presented in Section 1. The analysis of the equivalent circuit of RLFWG-SWS is given in Section 2. The FWG-SWS, as a special case of RLFWG-SWS, which can be formed by changing the height of the ridge of RLFWG-SWS, is also discussed in this Section. The

numerical analysis of high-frequency characteristics of RLFWG-SWS and FWG-SWS are given in Section 3. A brief summary is given in Section 4.

2. EQUIVALENT CIRCUIT OF RLFWG-SWS

The circuit is formed by the *E*-plane bend of a folded rectangular waveguide. The ridges are loaded on the straight portions of FWG-SWS to increase the longitudinal electric field in the beam tunnel. It is assumed that the lowest transverse electric mode, TE_{10}, propagates along the fold path shown by dotted line in Figure 1(a). An electron beam passes through a small hole on the broad wall of the serpentine waveguide where the electric field intensity peaks. The beam-wave interaction in RLFWG-SWS occurs when a beam phase velocity is synchronized with the effective slow-down wave phase velocity. Figure 1(b) shows the transverse dimensions of the RLFWG-SWS. According to transmission line theory, it is feasible that the ridge-loaded folded waveguide can be modeled with an equivalent circuit, which is shown in Figure 2.

The RLFWG-SWS can be represented by different circuit components, which have their own transfer matrix [23]. Since folded waveguide is a periodic structure, the circuit parameters can be treated only with one pitch, the analytical model of the ridge-loaded folded waveguide is divided into six parts.

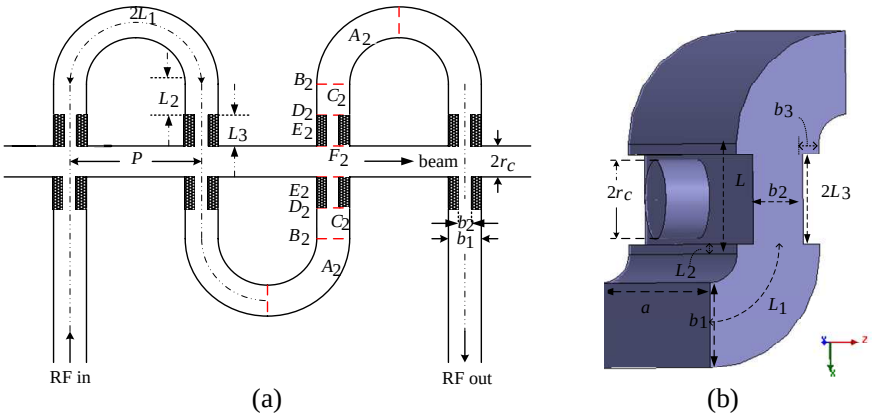

Figure 1. (a) Illustrative sketch of the RLFWG-SWS showing the relevant dimensions. (b) 3-D structure of RLFWG-SWS and the parameters of this structure are shown in Table 1.

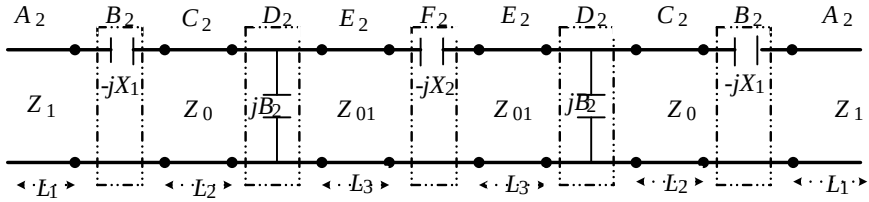

Figure 2. A periodic equivalent circuit model of RLFWG-SWS.

Table 1. Parameters of the RLFWG-SWS.

Parameter	Value (mm)
waveguide broad wall dimension a	2.96
narrow dimension of the waveguide b	0.65
the length of the straight waveguide L	0.8
the length of the pitch of the RLFWG-SWS p	0.88
the radius of the beam tunnel r_c	0.25
thickness of the ridge b_3	$0.2b$
height of the ridge $2L_3$	L

A_2) a uniform circular E-plane bending of rectangular waveguide;
C_2) straight rectangular waveguide;
B_2) an E-plane junction of the straight rectangular waveguide and a uniform circular bend of rectangular waveguide;
E_2) another straight rectangular waveguide, which change the narrow dimension basis of the former straight rectangular waveguide;
D_2) the junction of the two straight rectangular;
F_2) electron beam-hole;
Each part has their own transfer matrix by use of the knowledge of microwave networks. It can be written as follows [23]

$$A_2 = \begin{pmatrix} \cos(\beta_1 L_1) & j\sin(\beta_1 L_1)\cdot Z_1 \\ j\sin(\beta_1 L_1)\cdot Y_1 & \cos(\beta_1 L_1) \end{pmatrix} \tag{1}$$

$$B_2 = \begin{pmatrix} 1 & -jX_1 \\ 0 & 1 \end{pmatrix} \tag{2}$$

$$C_2 = \begin{pmatrix} \cos(\beta_0 L_2) & j\sin(\beta_0 L_2)\cdot Z_0 \\ j\sin(\beta_0 L_2)\cdot Y_0 & \cos(\beta_0 L_2) \end{pmatrix} \tag{3}$$

$$D_2 = \begin{pmatrix} 1 & 0 \\ jB_2 & 1 \end{pmatrix} \tag{4}$$

$$E_2 = \begin{pmatrix} \cos(\beta_0 L_3) & j\sin(\beta_0 L_3)\cdot Z_{01} \\ j\sin(\beta_0 L_3)\cdot Y_{01} & \cos(\beta_0 L_3) \end{pmatrix} \tag{5}$$

$$F_2 = \begin{pmatrix} 1 & -jX_2 \\ 0 & 1 \end{pmatrix} \tag{6}$$

where, β_0 is the axial propagation constant of the straight waveguide (C_2) and (E_2) and β_1 the axial propagation constant of the uniform circular bend of rectangular cross section waveguide (A_2). L_1, L_2, L_3 are the path length for the electromagnetic wave in the waveguide (A_2), (C_2) and (E_2), respectively. The straight waveguide (C_2) is treated as uniform transmission line with characteristics impedance of Z_0 and wave admittance of Y_0. While the serpentine E-plane bend waveguide (A_2), is also considered to uniform transmission line and has the characteristics impedance Z_1 and wave admittance Y_1. Meanwhile, E_2 is treated as uniform transmission line with characteristics impedance of Z_{01} and wave admittance of Y_{01}. The discontinuity (B_2) between serpentine E-plane bending waveguide (A_2) and straight waveguide (C_2) is represented by series reactance X_1.The discontinuity (D_2) between straight waveguide (C_2) and straight waveguide (E_2) is represented by shunt admittance B_2 and the beam-hole on the straight waveguide is represented by series reactanceX_2.

Expressions for the parameters in the above matrixes are given as [23, 24]

$$\frac{Z_1}{Z_0} = 1 + \frac{1}{24}\left(\frac{2b_1}{p}\right)^2 - \frac{1}{60}\left(\frac{2b_1}{p}\right)^2\left(\frac{2\pi b_1}{\lambda_g}\right)^2 \tag{7}$$

$$\frac{X_1}{Z_0} = \frac{32}{\pi^2}\left(\frac{2\pi b_1}{\lambda_g}\right)^3\left(\frac{2b_1}{p}\right)^2 \sum_{n=1,3,\ldots}^{\infty} \frac{1}{n}\sqrt{1-\left(\frac{2b_1}{n\lambda_g}\right)^2} \tag{8}$$

$$\frac{X_2}{Z_{01}} = \frac{1}{4\pi^2}\beta_0 b_2\left(\frac{a}{b_2}\right)^2\left(\frac{2r_c}{a}\right)^3 \tag{9}$$

$$\lambda_g' = \lambda_g\left\{1 + \frac{1}{12}\left(\frac{2b_1}{p}\right)^2\left[\frac{1}{2} - \frac{1}{5}\left(\frac{2\pi b_1}{\lambda_g}\right)^2\right]\right\} \tag{10}$$

$$Z_{01} = \frac{b_2}{b_1}Z_0 \tag{11}$$

$$\frac{B_2}{Y_0} = \frac{2b_1}{\lambda_g}\ln\csc\left(\frac{\pi b_2}{2b_1}\right) \tag{12}$$

Here, p is the pitch of the RLFWG-SWS, b_2 the narrow dimension of the waveguide (E_2), and λ'_g the guide-wavelength of the circular bend of rectangular cross section waveguide (A_2). a is waveguide broad wall dimension, b_1 the narrow dimension of the waveguide (C_2), λ the free space wavelength, λ_g the guide-wavelength of straight waveguide (C_2) and (E_2), and r_c the tunnel radius.

3. ANALYSIS OF HIGH-FREQUENCY CHARACTERISTICS OF RLFWG-SWS

3.1. Dispersion Relation

Treating the entire folded waveguide as a single transmission line, the transfer matrix H for one pitch of the circuit can be obtained by serial multiplication of the individual transfer matrix. Since the cascaded matrix is solvable, the high frequency characteristics of the RLFWG-SWS can be determined.

For the single equivalent matrix, the following expressions can be obtained according to [24]

$$\begin{bmatrix} V_1 \\ I_1 \end{bmatrix} = [H] \begin{bmatrix} V_2 \\ I_2 \end{bmatrix} \tag{13}$$

where

$$H = \begin{bmatrix} \cos\kappa & jZ\sin\kappa \\ jY\sin\kappa & \cos\kappa \end{bmatrix} \tag{14}$$

Here, V_1 and V_2 are the voltages at the output and input of the equivalent transmission line, respectively. κ is the phase shift. Y and Z are the admittance and impedance of the FWG equivalent circuit, respectively.

As discussed above, the cascaded product of these individual circuit can be equated to the single equivalent transmission line matrix $[H]$.

$$H = [A_2][B_2][C_2][D_2][E_2][F_2][E_2][D_2][C_2][B_2][A_2] \tag{15}$$

Substituting (1)–(6) into (15), the dispersion relation can be obtained, which can be written as

$$\begin{aligned} &\cos\kappa_1 \\ &= \frac{1}{2}(1+M_3)M_9 + \frac{Y_1Z_0^2}{4}M_7M_{10} + \frac{X_1Y_1}{2}M_2M_9 + \frac{X_1B_2}{2}M_5M_9 \\ &\quad + \frac{Y_1Z_0^2B_2}{4}M_7M_9 + \left(\frac{X_1^2Y_0Y_1}{4} - \frac{Y_0Z_1}{4} - \frac{X_1Y_1Z_0B_2}{2} - \frac{Y_1Z_0}{4}\right)M_4M_9 \end{aligned}$$

$$+\left(\frac{X_1^2Y_1B_2}{2}-\frac{B_2Z_1}{4}\right)M_6M_9-\frac{Z_0}{2}M_1M_{10}+\frac{X_1}{2}M_5M_{10}$$
$$+\left(\frac{X_1^2Y_1}{4}-\frac{Z_1}{4}\right)M_6M_{10}+\left(\frac{X_1Y_0}{2}-\frac{B_2Z_0}{2}\right)M_1M_9-\frac{X_1Y_1Z_0}{2}M_4M_{10} \quad (16)$$

$$\cos\kappa_2$$
$$=\left(\frac{Y_0}{2}+\frac{B_2X_1Y_0}{2}\right)M_1M_{11}+\frac{X_1Y_0^2}{2}M_8M_{11}-\frac{B_2}{2}(1-M_3)M_{11}$$
$$+\frac{B_2X_1Y_1}{2}M_2M_{11}+\left(\frac{X_1Y_1Y_0}{2}-\frac{B_2Z_1Y_0}{4}+\frac{X_1^2B_2Y_0Y_1}{4}-\frac{B_2Z_0Y_1}{4}\right)M_4M_{11}$$
$$+\left(\frac{X_1^2Y_1Y_0^2}{4}-\frac{Y_0^2Z_1}{4}\right)M_7M_{11}+\frac{Y_1}{4}M_6M_{11}+\frac{X_1Y_0}{2}M_1M_{12}$$
$$-\frac{1}{2}(1-M_3)M_{12}+\frac{X_1Y_1}{2}M_2M_{12}+\left(\frac{X_1^2Y_1Y_0}{4}-\frac{Y_0Z_1}{2}\right)M_4M_{12} \quad (17)$$

$$\cos\kappa$$
$$=\cos\kappa_1+\cos\kappa_2 \quad (18)$$

where, $\beta_0=\frac{2\pi}{\lambda_g}$, $\beta_1=\frac{2\pi}{\lambda_g'}$, and

$$M_1=\sin 2(\beta_0L_2)\cos 2(\beta_1L_1)$$
$$M_2=\cos 2(\beta_0L_2)\sin 2(\beta_1L_1)$$
$$M_3=\cos 2(\beta_0L_2)\cos 2(\beta_1L_1)$$
$$M_4=\sin 2(\beta_0L_2)\sin 2(\beta_1L_1)$$
$$M_5=\cos 2(\beta_1L_1)+M_3$$
$$M_6=\sin 2(\beta_1L_1)+M_2$$
$$M_7=\sin 2(\beta_1L_1)-M_2$$
$$M_8=\cos 2(\beta_1L_1)-M_3$$
$$M_9=\cos 2(\beta_0L_3)+\left(\frac{X_2Y_0}{2}-B_2Z_{01}\right)\sin 2(\beta_0L_3)+B_2X_2\cos^2(\beta_0L_3)$$
$$M_{10}=B_2\cos 2(\beta_0L_3)+\left(\frac{B_2X_2Y_{01}}{2}+Y_{01}\right)\sin 2(\beta_0L_3)+X_2Y_{01}^2\sin^2(\beta_0L_3)$$
$$M_{11}=X_2\cos^2(\beta_0L_3)-Z_{01}\sin 2(\beta_0L_3)$$
$$M_{12}=\cos 2(\beta_0L_3)+\frac{X_2Y_{01}}{2}\sin 2(\beta_0L_3)$$

We can obtain the dispersion relation by solving the Equations (16)–(18). The effective phase shift per period of the structure, as seen by the electron beam, is given by

$$\beta=\frac{\kappa+\pi}{p}=\frac{\arccos(\cos\kappa_1+\cos\kappa_2)+\pi}{p} \quad (19)$$

Here, the additional π term accounts for the inherent 180° phase shift of the electric field with respect to the electrons in one period, due to the folded nature of the RLFWG-SWS.

The phase velocity as seen by electrons can be obtained as follows: $v_p = \frac{\omega}{\beta}$.

3.2. Interaction Impedance

The on-axis interaction impedance of the RLFWG-SWS can be obtained as following expressions which stem from R. G. E. Hutter [25].

$$k_c = Z_{01}\left[\frac{1}{\beta_0 p}\right]^2\left[\frac{\sin\frac{\beta_0 b_2}{2}}{\frac{\beta_0 b_2}{2}}\right]^2\frac{1}{I_0^2(\tau r_c)} \tag{20}$$

$$Z_{01} = 120\pi\frac{2b_2}{a}\frac{\lambda_g}{\lambda} \tag{21}$$

$$\tau^2 = \beta_0^2 - \left(\frac{\omega}{c}\right)^2 \tag{22}$$

where ω is the angular frequency of the wave (rad/s), c the speed of light, and I_0 a modified Bessel function.

3.3. Analysis of FWG-SWS

The FWG-SWS is a special case of RLFWG-SWS, which can be formed if L_3 is equal to zero. In the particular case, both D_2 and E_2 circuits vanished. A periodic equivalent circuit model of FWG-SWS is shown as Figure 3. It is particular note that the discontinuity of the beam-hole on the straight waveguide is represented by series reactance X_2, which is different from the beam-hole having been represented by π type network [12].

The high-frequency characteristics of SFWG-SWS are analyzed by the means of the same approach as the RLFWG-SWS.

Based on the above analysis of RLFWG-SWS, the dispersion relation and interaction impedance can be written as:

$$\begin{aligned}\cos\kappa = T_1 + [\frac{X_1X_2}{2Z_0Z_1} + \frac{X_1^2}{2Z_0Z_1} - \frac{1}{2}(\frac{Z_0}{Z_1} + \frac{Z_1}{Z_0})]T_2 + (\frac{X_1}{Z_0} + \frac{X_2}{2Z_0})T_3 \\ + \frac{X_1}{Z_1}T_4 + \frac{X_2}{4Z_1}T_5 + \frac{X_1X_2}{2Z_0^2}T_6 + (\frac{X_1^2X_2}{4Z_0^2Z_1} - \frac{X_2Z_1}{4Z_0^2})T_7\end{aligned} \tag{23}$$

$$k_c = Z_0\left[\frac{1}{\beta p}\right]^2\left[\frac{\sin\frac{\beta b}{2}}{\frac{\beta b}{2}}\right]^2\frac{1}{I_0^2(\tau r_c)} \tag{24}$$

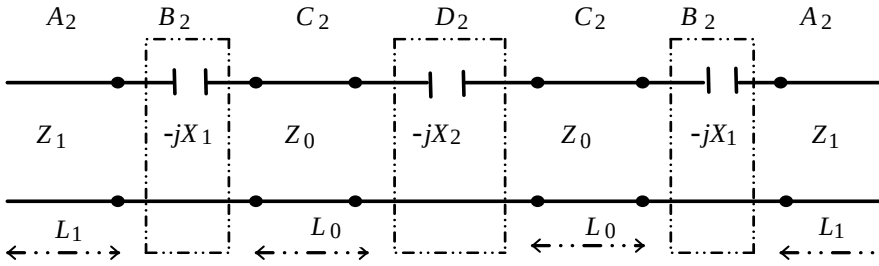

Figure 3. An equivalent circuit model of FWG-SWS.

where

$$\begin{aligned}
T_1 &= \cos 2(\beta_0 L_0)\cos 2(\beta_1 L_1) \\
T_2 &= \sin 2(\beta_0 L_0)\sin 2(\beta_1 L_1) \\
T_3 &= \sin 2(\beta_0 L_0)\cos 2(\beta_1 L_1) \\
T_4 &= \cos 2(\beta_0 L_0)\sin 2(\beta_1 L_1) \\
T_5 &= \sin 2(\beta_1 L_1) + T_4 \\
T_6 &= \cos 2(\beta_1 L_1) - T_1 \\
T_7 &= \sin 2(\beta_1 L_1) - T_4
\end{aligned}$$

4. RESULTS OF NUMERICAL CALCULATIONS

The dispersion relation (19) and the interaction impedance (20) in the previous section can be solved numerically. For comparison, we also simulated the structure using 3-D electromagnetic code HFSS where the circuit has been considered to be lossless.

Figure 4 shows the dispersion relation and interaction impedance of RLFWG-SWS. In Figure 4(a), the values of normalized phase velocity calculated in each model differ from each other by an average of 0.79%. As can be seen in Figure 4(b), there is fairly good agreement between two models. The greatest variation in estimated impedance seems to be at the lower band edge, which is far from the center frequency. Both dispersion relation and interaction impedance obtained by equivalent circuit have some difference from HFSS. This is because that all the discontinuities in the RLFWG-SWS are represented by various lumped parameters and the accuracy rely on the ratio of tunnel radius to narrow dimension of waveguide.

In order to study the high-frequency characteristics of RLFWG-SWS more specifically, the influences of the ridge dimensions on dispersion relation and interaction impedance are investigated. It is

shown in Figure 5 that, with the ridge thickness increases, the relative passband decreases rapidly and the interaction impedance increases noticeably. But we should choose the properly thickness of the ridge considering both passband and interaction impedance. Figure 6 shows that the effect on high-frequency characteristics by changing the height of the ridge. It can be concluded that, with the increase of L_3, the normalized phase velocity decreases, the relative passband becomes narrow and the interaction impedance increases. It is important to note that the impedance increases slowly particularly as L_3/L is greater

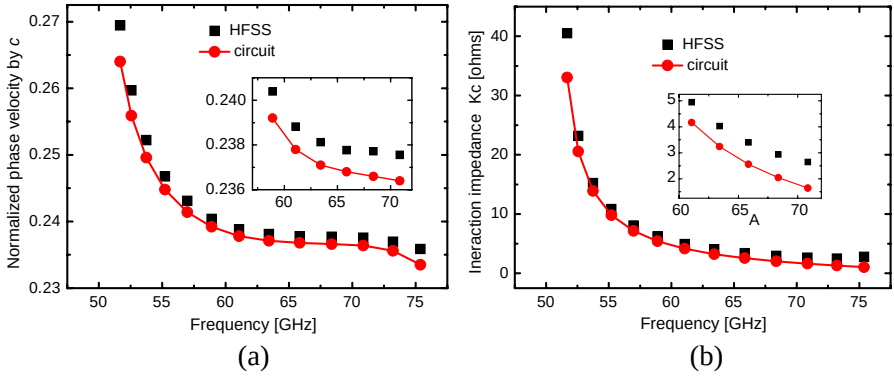

Figure 4. (a) Plot of effect axial normalized phase velocity versus frequency, comparing equivalent circuit and HFSS models. (b) Plot of on-axis interaction impedance versus frequency, comparing equivalent circuit and HFSS models.

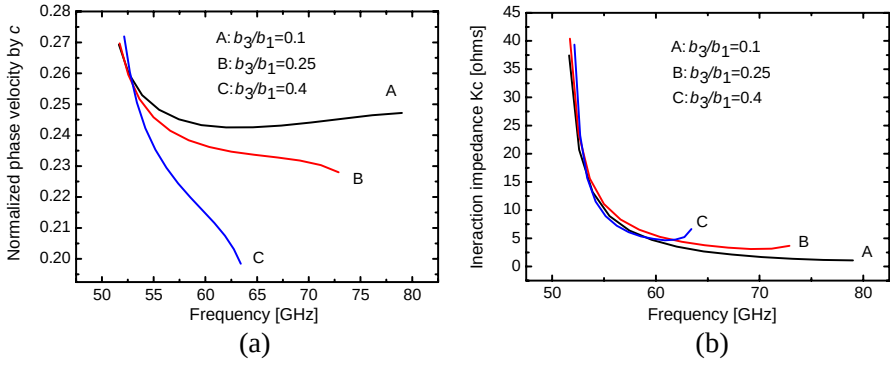

Figure 5. (a) Effect of the ridge thickness b_3 on the normalized phase velocity. (b) Effect of the ridge thickness b_3 on the interaction impedance.

than 0.4.

The dispersion relation (23) and the interaction impedance (24) of FWG-SWS also can be numerical calculated. We used four kinds of method to analyze the FWG-SWS, including the equivalent circuit approaches reported in references [12] and [16], HFSS, and the present method. The numerical calculation results are shown in Figure 7. It is indicated that the other three calculation data agree well with the numerical calculation data from the present method, which support our theory and show that the present method is reliable. On the other hand, since the present method is analytic, it is easier to work into an optimization algorithm and is faster to compute as long as given the parameters of FWG-SWS without setting a model. This means that

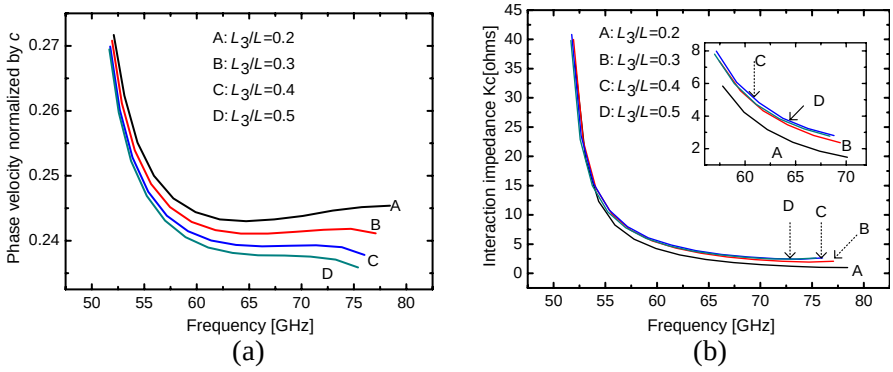

Figure 6. (a) Effect of the ridge height L_3 on the normalized phase velocity. (b) Effect of the ridge thickness L_3 on the interaction impedance.

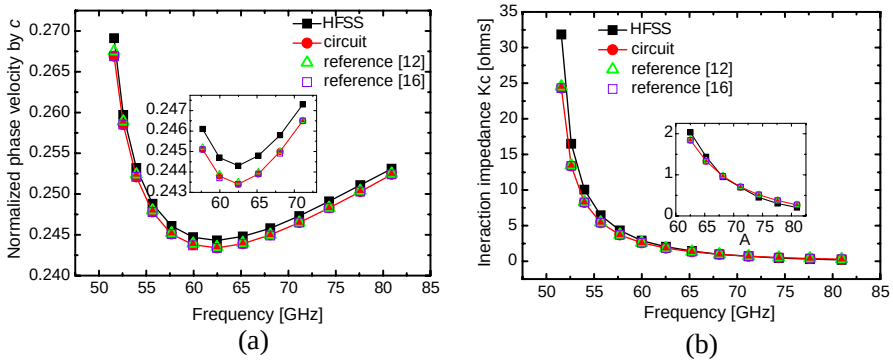

Figure 7. (a) Plot of effect axial normalized phase velocity versus frequency, comparing various models. (b) Plot of on-axis interaction impedance versus frequency, comparing various models.

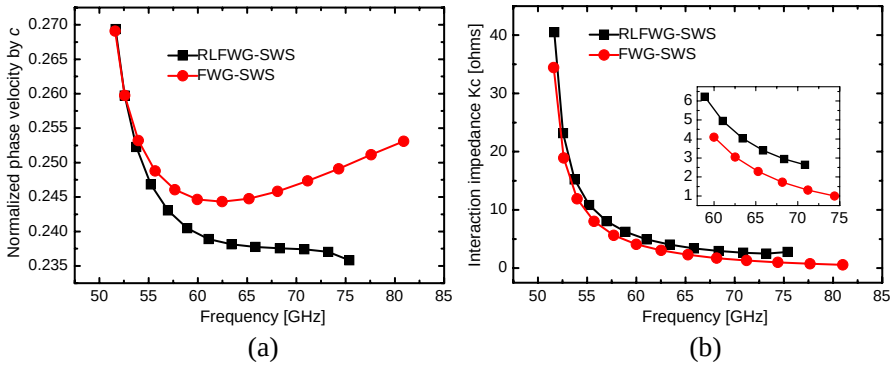

Figure 8. (a) Plot the dispersion relation of RLFWG-SWS and FWG-SWS basis of the same dimensions, respectively. (b) Plot the interaction impedance of RLFWG-SWS and FWG-SWS basis of the same dimensions, respectively.

the present method is high efficiency.

Figure 8 shows that the effect of ridge-loaded on the dispersion relation and interaction impedance. It is observed that the RLFWG-SWS have lower normalized phase velocity and higher interaction impedance than FWG-SWS.

5. CONCLUSION

In this paper, an equivalent circuit approach of RLFWG-SWS is proposed. Unlike time-consuming 3-D electromagnetic simulation software, the present analysis is simple and provides closed-form expressions for obtaining the dispersion and the interaction impedance characteristics of the structure. It is found that the analysis results based on the equivalent circuit fairly agree with the results obtained by HFSS.

Such a circuit analysis is quite useful as a design tool which is easier to carry out an optimization algorithm with high efficiency, particularly for rapid parametric studies in the early phase of the design. The explicit relations between the design parameters provide physical insights into the dependence of the device performance on the structures parameters. Moreover, this method has several merits such as simple, fast, sufficient accurate and etc. In the future, in order to increase the electron efficiency of the interaction, it is feasible to search other novel slow-wave structures which are related to SFWG-SWS. By means of the equivalent circuit approach, we also can analyze these

novel slow-wave structures which have more complicated boundary conditions than conventional SFWG-SWS. Subsequently, we plan to analyze the ridge-vane loaded folded waveguide slow-wave structure and the related analysis is in progress.

ACKNOWLEDGMENT

This work was supported by the National Science Fund for Distinguished Young Scholars of China (Grant No. 61125103), the Vacuum Electronics National Lab Foundation, China (Grant No. 9140C050101110C0501), the National Natural Science Foundation of China (Grant Nos. 60971038 and 60971031) and the Fundamental Research Funds for the Central Universities, China (Grant Nos. ZYGX2010J1054 and ZYGX2011J034).

REFERENCES

1. Döhler, G., D. Gagne, D. Gallagher, and R. Moats, "Serpentine wave-guide TWT," *1987 International Electron Devices Meeting Technical Digest*, Vol. 33, 485–488, 1987.
2. Kesari, V., "Beam-absent analysis of disc-loaded-coaxial waveguide for application in gyro-TWT (Part-1)," *Progress In Electromagnetics Research*, Vol. 109, 211–227, 2010.
3. Kesari, V., "Beam-present analysis of disc-loaded-coaxial waveguide for its application in gyro-TWT (Part-2)," *Progress In Electromagnetics Research*, Vol. 109, 229–243, 2010.
4. Kesari, V. and J. P. Keshari, "Analysis of a circular waveguide loaded with dielectric and metal discs," *Progress In Electromagnetics Research,* Vol. 111, 253–269, 2011.
5. Mustafa, F. and A. M. Hashim, "Properties of electromagnetic fields and effective permittivity excited by drifting plasma waves in semiconductor-insulator interface structure and equivalent transmission line technique for multi-layered structure," *Progress In Electromagnetics Research*, Vol. 104, 403–425, 2010.
6. Duan, Z., Y. Wang, X. Mao, W.-X. Wang, and M. Chen, "Experimental demonstration of double-negative metamaterials partially filled in a circular waveguide," *Progress In Electromagnetics Research*, Vol. 121, 215–224, 2011.
7. Kuo, C.-W., S.-Y. Chen, Y.-D. Wu, and M.-H. Chen, "Analyzing the multilayer optical planar waveguides with double-negative metamaterial," *Progress In Electromagnetics Research*, Vol. 110, 163–178, 2010.

8. Choi, J. J., C. M. Armstrong, F. Calise, A. K. Ganguly, R. H. Kyser, G. S. Park, R. K. Parker, and F. Wood, "Experimental observation of coherent millimeter wave radiation in a folded waveguide employed with a gyrating electron beam," *Phys. Rev. Lett.*, Vol. 76, No. 22, 4273–4276, May 1996.
9. Kory, C., J. David, H. T. Tran, L. Ives, and D. Chernin, "Folded waveguide circuit optimizations using Christine 1D," *Proc. 32nd IEEE Int. Conf. Plasma Sci.*, 333, Jun. 2005.
10. Booske, J. H., "New opportunities in vacuum electronics through the application of microfabrication technologies," *Proc. Int. Vac. Electron. Conf.*, 11–12, Apr. 2002.
11. Han, S. T., K. H. Jang, J. K. So, J. I. Kim, Y. M. Shin, N. M. Ryskin, S. S. Chang, and G. S. Park, "Low-voltage operation of Ka-band folded waveguide traveling-wave tube," *IEEE Trans. Plasma Sci.*, Vol. 32, No. 1, 60–66, Feb. 2004.
12. Booske, J. H., M. C. Converse, C. L. Kory, C. T. Chevalier, D. A. Gallagher, K. E. Kreischer, V. O. Heinen, and S. Bhattacharjee, "Accurate parametric modeling of folded waveguide circuits for millimeter-wave traveling wave tubes," *IEEE Trans. Electron. Devices*, Vol. 52, No. 5, 685–694, May 2005.
13. Han, S. T., J. I. Kim, K. H. Jang, J. K. So, S. S. Chang, N. M. Ryskin, and G. S. Park, "Experimental investigation of millimeter wave folded-waveguide TWT," *Proc. Int. Vac. Electron. Conf.*, 322–323, May 2003.
14. He, J., Y. Wei, Z. Lu, et al., "Investigation of a ridge-loaded folded waveguide slow-wave system for the millimeter wave traveling wave tube," *IEEE Trans. Plasma Sci.*, Vol. 38, No. 7, 1556–1562, 2010.
15. Liu, S., "Folded waveguide circuit for broadband MM wave TWTs," *Int. J. Infrared Millim Waves*, Vol. 16, 809–815, 1995.
16. Na, Y. H., S. W. Chung, and J. J. Choi, "Analysis of a broadband Q-band folded-waveguide traveling-wave tube," *IEEE Trans. Plasma Sci.*, Vol. 30, 1017–1022, 2002.
17. Han, S.-T., J.-I. Kim, and G. S. Park, "Design of a folded waveguide traveling-wave tube," *Microw Opt. Technol. Lett.*, Vol. 38, 161–165, 2003.
18. Sumathy, M., K. J. Vinoy, and S. K. Datta, "Analysis of ridge-loaded folded-waveguide slow-wave structures for broadband traveling-wave tubes," *IEEE Trans. Electron. Devices*, Vol. 57, No. 6, 1440–1446, Jun. 2010.
19. Liu, Y., J. Xu, Y.-Y. Wei, X. Xu, F. Shen, M. Huang, T. Tang,

W.-X. Wang, Y.-B. Gong, and J. Feng, "Design of a V-band high-power sheet-beam coupled-cavity traveling-wave tube," *Progress In Electromagnetics Research*, Vol. 123, 31–45, 2012.

20. Tahir, F. A., H. Aubert, and E. Girard, "Equivalent electrical circuit for designing mems-controlled reflectarray phase shifters," *Progress In Electromagnetics Research*, Vol. 100, 1–12, 2010.
21. Klopf, E. M., S. B. Manić, M. M. Ilić, and B. M. Notaroš, "Efficient time-domain analysis of waveguide discontinuities using higher order FEM in frequency domain," *Progress In Electromagnetics Research*, Vol. 120, 215–234, 2011.
22. *High Frequency Structure Simulator User's Reference,* Ansoft Corp., Pittsburgh, PA, 2001.
23. Collin, R. E., *Foundations for Microwave Engineering,* Wiley-IEEE Press, New York, 2000.
24. Marcuvitz, N., *Waveguide Handbook,* McGraw-Hill, New York, 1951.
25. Hutter, R. G. E., *Beam and Wave Electronics in Microwave Tubes,* Van Nostrand, New York, 1960.